Materials Advances

ROYAL SOCIETY OF CHEMISTRY

PAPER

View Article Online
View Journal | View Issue

Cite this: *Mater. Adv.*, 2026, 7, 1311

Porous graphite plate design in SiC PVT growth: optimized powder source evolution for enhanced crystal yield and quality

Yang Chen,[a] Xiaofang Ye,[a] Shilin Liu,[a] Wenyu Kang,*[a] Wei Jiang,[a] Jun Yin*[a] and Junyong Kang[ab]

Received 30th October 2025,
Accepted 9th December 2025

DOI: 10.1039/d5ma01254f

rsc.li/materials-advances

The third-generation semiconductor, silicon carbide (SiC), has become increasingly crucial in emerging markets for radio-frequency and power electronic devices due to its superior physical properties. However, the insufficient growth thickness and low powder source utilization rate still limit the development of physical vapor transport (PVT) growth. In this work, a systematic investigation on the evolution progress and consumption features of the SiC powder source in PVT growth was conducted by theoretical simulations and experimental measurements. We found that the non-uniform source consumption and recrystallization negatively impacted the evolution of thermal and flow fields, resulting in a final low utilization rate of the powder source. To enhance the usage of the powder source and the quality of as-grown crystals, we designed a porous graphite plate in the PVT chamber to modulate both mass transfer processes and the thermal field. Compared to a conventional structure, the designed porous graphite plate could optimize the utilization rate (29% enhanced) and the spatial uniformity of source consumption, thereby increasing the crystal growth rates by 33%. Meanwhile, this designed plate could reduce the thermal stress gradients and thus reduce the defect density (52%) within the SiC crystals.

1. Introduction

Silicon carbide (SiC) has attracted significant attention in emerging applications such as new energy vehicles, renewable energy inverters, 5G communications, and military-grade electronics due to its exceptional physical properties,[1–3] including a wide bandgap, high breakdown electric field strength, superior thermal conductivity, and high saturated electron drift velocity.[4–6] Physical vapor transport (PVT) is the main method for industrial-scale SiC production, owing to its low capital expenditure, simplified system architecture, and proven technological maturity. However, reconciling the competing requirements of cost efficiency, wafer-size scalability, and defect-free crystalline quality is the foremost challenge in PVT-grown SiC single crystals.

Conventional PVT growth of SiC single crystals relies on the thermal decomposition and sublimation of the powder source material. The resultant vapor species (primarily Si/C-containing gases) are transported along a temperature gradient to a low-temperature seed crystal, and then undergo adsorption and crystallization. The necessary axial temperature gradient in the growth chamber results in an inconsistent consumption of the powder source and a partial recrystallization in the lower-temperature region during the crystal growth process.[7] This further leads to a non-uniform source consumption and a low source utilization rate, which subsequently and negatively influence the axial growth thickness and crystalline perfection. To address these challenges, researchers have explored multiple strategies to homogenize source consumption and improve crystal quality. Tan *et al.* developed a gas deflector within the growth chamber to suppress convection, ensuring more uniform gas-phase material transport, which in turn improved the crystal quality and yield.[8] Wang *et al.* achieved faster growth rates by optimizing the source material's packing density, enabling consistent sublimation.[9] Chao *et al.* enhanced the crystal quality by integrating graphite rings onto the source chamber surface and adding graphite blocks, effectively reducing crystal defects and preventing polycrystallization.[10] Zhang *et al.* demonstrated that modifying the thickness and spatial arrangement of thermal insulation felts helped maintain uniform source sublimation while supporting a microscale convex

[a] *Pen-Tung Sah Institute of Micro-Nano Science and Technology, Engineering Research Center of Micro-Nano Optoelectronic Materials and Devices, MOE, College of Physical Science and Technology, Tan Kah Kee Innovation Laboratory (FDIX), Xiamen University, Xiamen 361005, China. E-mail: wykang@xmu.edu.cn, jyin@xmu.edu.cn*
[b] *Hefei National Laboratory, Hefei 230088, China*

growth interface.[11] Other techniques that modify the thermal field of the growth equipment have also been reported. Recent work by Nakamura *et al.* demonstrated that system-level reconstruction of the thermal field can effectively improve powder-source utilization.[12] Liu *et al.* increased the sublimation rate by modulating the relative positioning of the induction coil and crucible.[7] Yang *et al.* reduced recrystallization losses by fine-tuning the heater coil's turns ratio, thereby improving source utilization efficiency.[13] Furthermore, replacing traditional powders with recycled CVD-SiC blocks has also proven effective in increasing the growth rate and quality of SiC single crystals.[14] Despite these advances, achieving uniform consumption of powder in the crucible and suppressing recrystallization in the upper area of the powder remains a major challenge. In addition, a synergistic optimization of mass transfer processes during the PVT growth is still required.

In this work, we conducted a comprehensive investigation of the evolution of the SiC powder source in PVT growth by multi-physics simulations and experimental measurements. The key evolutionary behaviours (including progressive consumption, graphitization, and recrystallization) were systematically analysed to elucidate their impact on mass transfer dynamics and crystal growth evolution. To address the limitations in the conventional PVT growth, a porous graphite (PG) plate was designed to optimize spatial consumption and mitigate recrystallization effects, thereby improving mass transfer processes.

2. Experimental details

2.1. Numerical simulation

The numerical simulation model for SiC PVT growth in this study was established based on parameters from our previous experiment on 150-mm 4H-SiC single-crystal growth, and the PVT system is illustrated in Fig. 1a. There were five main parts in this PVT system, including a thermal insulation felt, graphite crucible, SiC seed crystal, SiC source material, and resistive heater. Under heating from the resistive heater, the SiC source material went through sublimation, producing vapor-phase species that ascend and crystallize onto the lower-temperature seed. Leveraging the axisymmetric geometry of the growth system, this work adopted a 2D axisymmetric numerical framework to enhance computational efficiency while maintaining physical fidelity. The multi-physics model was implemented using COMSOL Multiphysics®, encompassing full-cycle simulation stages from geometric modelling and coupled physics computation to result analysis.

The multi-physics model in this study coupled conjugate heat transfer, surface radiation, laminar flow, low-concentration species transport in porous media, and solid mechanics to construct a full-process simulation model. The detailed multi-physics model and parameters can be found in the Theoretical simulation model section in the SI. Experimental validation guided parameter calibration, requiring adjustment of the resistive-heater power to maintain a seed surface temperature of 2220 °C under an argon pressure of 5 Torr (Fig. 1b). The SiC

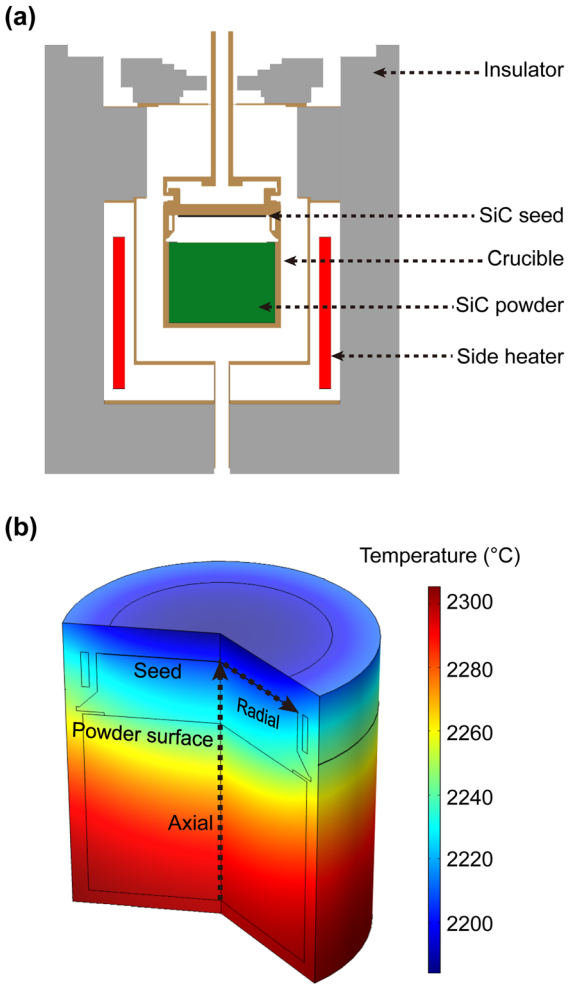

Fig. 1 (a) Schematic illustration of the 150-mm PVT growth system; (b) 3D-temperature distribution in the crucible during the growth.

powder source material (particle diameter of 1 mm with a porosity of 0.65) was modelled as distinct porous media domains.

2.2. Materials

The SiC powder source employed in this study consisted of high-purity granules packed within a 6-inch (150 mm) crystal growth furnace. The residual powder source went through a 40-hour PVT growth process at approximately 2200 °C seed temperature under a 5 torr Ar atmosphere. After the subsequent controlled cooling procedure, the residual powder source (which became a solid bulk after the sintering) in the crucible was sectioned transversely using a steel blade.

2.3. Micro-CT scanning

Micro-computed tomography (micro-CT) of the residual powder source after 40 hours of growth was performed using a commercial high-resolution industrial micro-CT system (Phoenix v|tome|x m, General Electric Company). During the scanning process, the sample was mounted on a rotating stage, and data were collected by step scanning with a rotation step of 0.3°, and

the X-ray exposure time for each projection was set to 2400 ms. The three-dimensional (3D) reconstruction of the semi-cylindrical SiC powder source was performed using VGStudio Max software (version 3.4).

2.4. XPS measurement

X-ray photoelectron spectroscopy (XPS) was used to perform elemental quantitative analysis of the powder source used for PVT growth of SiC single crystals. The particle samples were completely crushed into dense powders using a mortar and a pestle and then fixed on carbon tape to ensure minimal surface contamination. Spectra were acquired using a Thermo Scientific ESCALAB Xi^+ spectrometer. Survey scans were collected for the Si 2p and C 1s core levels. Charge neutralization was applied using a low-energy electron flood gun to compensate for sample charging. Quantitative atomic concentrations were calculated from the integrated peak areas of the core-level spectra, utilizing instrument-specific sensitivity factors and accounting for the inelastic mean free path (IMFP) of the photoelectrons.

3. Results and discussion

3.1. Revealing source evolution in conventional PVT growth

A multi-physics simulation framework was established to investigate the temporal evolution of thermal fields, gas-phase transport, and source material consumption during PVT growth. A constant temperature (about 2220 °C) at the crystal growth interface was fixed throughout simulations, consistent with actual crystal growth conditions. After a 168-hour growth, the temperature distribution within the source compartment changed significantly compared with the initial stage (*i.e.*, the 0 hour), as shown in Fig. 2a. The axial temperature profiles along the crucible centerline (Fig. S1a) showed a 15 °C decrease at the source bottom. This decrease might be caused by the severe graphitization of the bottom powder at high temperature, which brought an additional insulation effect. For the radial temperature distribution, a reduced surface temperature of the source material was found as the growth time increased (Fig. S1b), and this reduction might be due to the partially graphitized source material near the heater and the recrystallized SiC source at the upper region.

The velocity field was further extracted for analysis (Fig. 2b and Fig. S1c, d), and the results revealed a distinct evolution of the flow regimes. At the initial stage (0 hour), a uniform gas flow was observed within the powder source and dominated by the sidewall-driven convection. Meanwhile, an approximately 10-time higher convection velocity was found in the growth chamber. After growing for 168 hours, the main convection region in the source chamber changed to the bottom region near the crucible wall, and the velocity also increased significantly. This was caused by the increased porosity of the source material near the crucible wall due to the severe graphitization[15] and also attributed to the reduced porosity at the upper center region of the source due to recrystallization. In addition, the convection in the growth chamber was suppressed (70% weakened) due to the recrystallization at the upper region of the SiC source. This suppressed vapor transport would limit the growth rate of the SiC crystal, as evidenced by the significantly reduced net flux of reactive vapor species (32% average flux reduction), such as SiC_2 (Fig. S2). This consistently altered vapor transport was not good for the growth of high-quality and thick SiC bulks, as well as the high utilization of the SiC powder source.

To understand the detailed evolution of the source along the growth process, the gasification/solidification rate, recrystallized/consumed powder source ratio, graphitized volume ratio, and source porosity were calculated (Fig. 2c). The gasification rate distribution demonstrated a 70% decline in the reaction rate at the source sidewalls and bottom from 0.12 mol m^{-3} s^{-1} (Fig. S3) to 0.035 mol m^{-3} s^{-1} at 168 hours. Concurrently, the negative gasification rate (presented as SiC formation) in the upper-central source chamber decreased by 74% from −0.15 mol m^{-3} s^{-1} to −0.039 mol m^{-3} s^{-1}, reflecting attenuated gaseous component generation due to insufficient source replenishment. The inhomogeneity of the gasification across the source cross-section persisted along with growth duration, as indicated by the value distribution of the nine points at the typical regions (marked as triangles) in Fig. 2d. The result indicated that continuous inhomogeneous gasification and solidification (recrystallization) existed in the source chamber. The recrystallized/consumed powder source ratio (Fig. 2e) showed a deteriorated high variation due to this high inhomogeneity of the gasification within the source chamber. As a result, loose graphite accumulated progressively on the sidewalls and bottom of the source chamber during growth, attaining 90 vol% in these regions by 168 hours, as seen from the graphite volume ratio distribution in the solid phase (Fig. 2c(iii)). This reduced the thermal conductivity of the crucible bottom, thereby diminishing upward heat transfer and weakening the axial temperature gradient and growth driving force.[16,17] The inhomogeneous gasification and solidification (recrystallization) within the source chamber further resulted in the spatial variation of source porosity. The porosity and SiC consumption profiles (Fig. 2c(iv)) indicated that 94% of the SiC source was depleted in the sidewall and bottom regions by 168 hours. The porosity in these zones approached 0.56 owing to SiC consumption and a large amount of graphite accumulation, restricting gaseous component convection primarily to the source periphery.[18]

To validate the simulation results, the graphitization feature of the SiC source was compared with the XPS experimental results based on the measured C/Si atomic ratio for the typical residual powder source sample. Fig. 3a displays the cross-sectional photograph of the residual source material from a 6-inch crystal after 40 hours of growth, where peripheral regions (sidewalls and base) had extensive dark, loose graphite clusters (partially exfoliated during sampling), while the up-centre region showed light-coloured dense SiC polycrystals due to recrystallization. Notably, the lower temperature in the source surface area caused the recrystallization effect. This effect obviously increased the source surface density after a

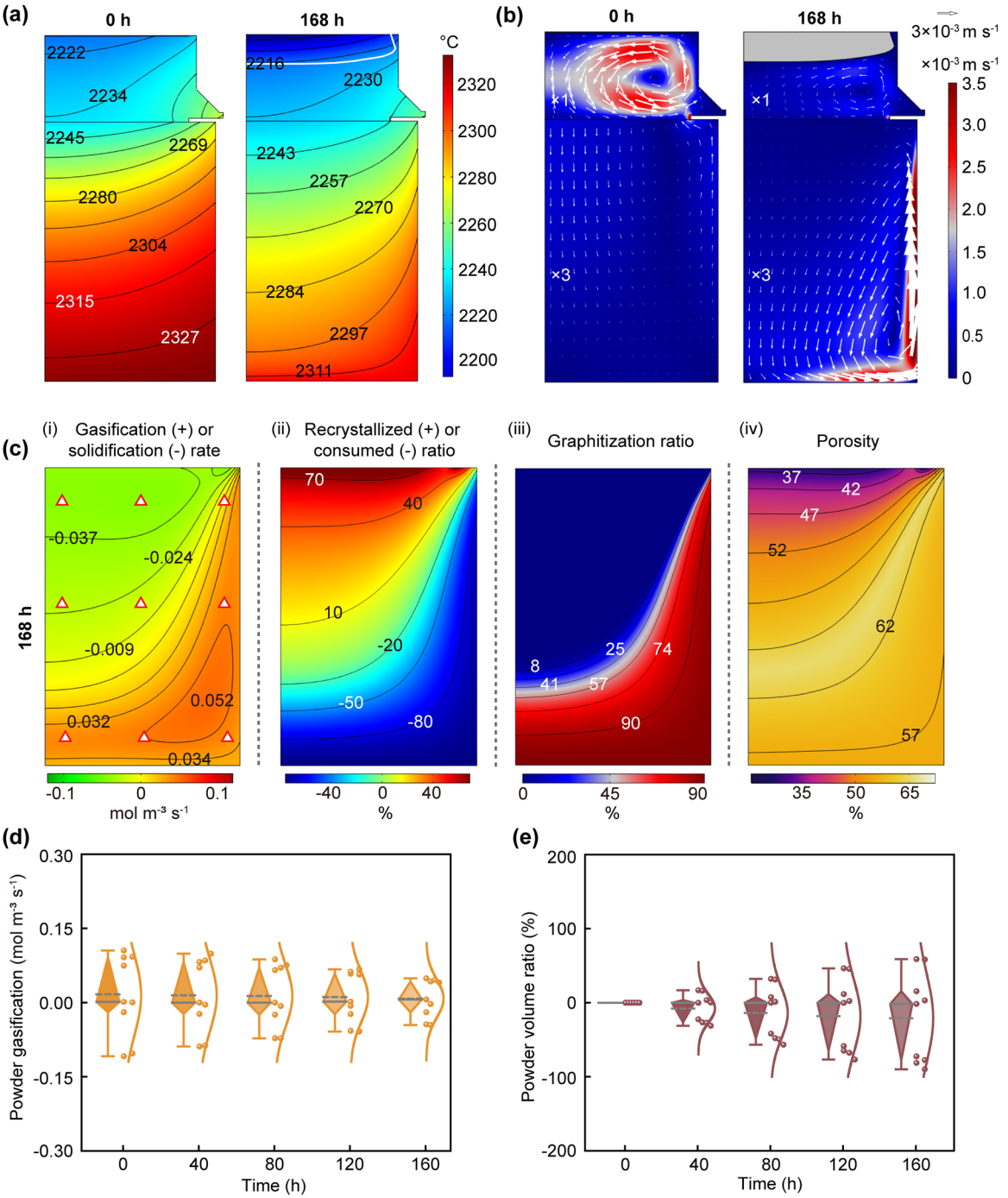

Fig. 2 (a) Simulated temperature distributions in the SiC growth crucible at 0 hour (left) and 168 hours (right). (b) The corresponding velocity fields at 0 hour (left) and 168 hours (right). The source chamber velocities were magnified 3× for clarity. (c) Distributions of the powder source (i) gasification (+) or solidification (−) rate, (ii) recrystallized (+) or consumed (−) volume ratio, (iii) graphitization volume ratio of the solid phase, and (iv) porosity after 168 hours of growth. (d) The violin plot distribution of the powder source gasification rate over time at 9 typical points (marked as white triangles shown in (c)-(i) in the powder source, with the dashed line representing the mean and the solid line representing the median. (e) The corresponding violin plot distribution of the powder source volume ratio over time for the 9 typical points.

period of growth. The measured C/Si atomic ratio distribution by XPS (Fig. S4) clearly confirmed the graphitized peripheral zones. The slightly higher C/Si ratios obtained at the source top relative to its center should have originated from the loose graphite particles entrained in the convective gas flows. The calculated graphite volume ratio is shown in Fig. 3b with a comparison of the simulation result. The results from the experimental and simulation data present a consistent trend in graphitization distribution, indicating that the theoretical simulation is reasonable and reliable.

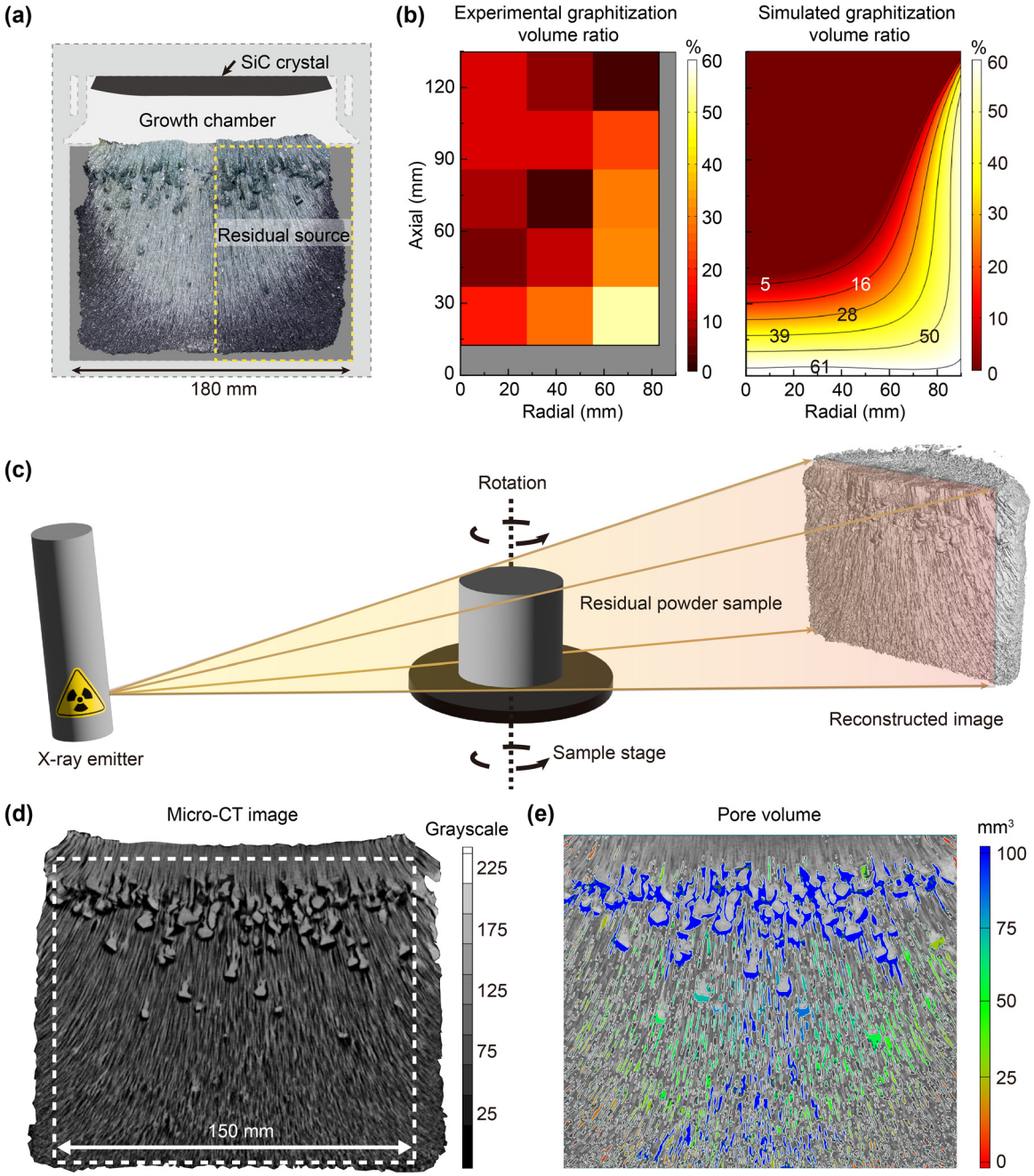

Fig. 3 (a) Cross-sectional photo image of the typical residual source material after 40-hour SiC growth. (b) Graphitization volume ratio of the powder source calculated by experiment and simulation (40 hours). (c) Illustration of the CT imaging and reconstruction of the residual powder source. (d) CT-based density mapping of the source material. (e) 3D-reconstructed pore volume distribution of the residual source material.

To obtain a more detailed picture of the powder source consumption during the growth process (including graphitization and recrystallization), the computed tomography (CT) imaging technology was introduced to observe the distribution of porosity and the density of the residual powder source after 40 hours of growth, and 3D reconstruction was performed (Fig. 3c). The typical cross-sectional CT tomographic image of the residual powder source is shown in Fig. 3d, and the full-scan vertical and horizontal cross-sectional CT images are presented in Videos S1 and S2. Based on the identification of the powder source morphology by the different density gray values (especially the pore area) the pore distribution diagram of the residual powder source could be easily derived from the CT image, as shown in Fig. 3e, and the full scan vertical and horizontal cross-sectional pore distribution diagrams are presented in Videos S3 and S4. In the graphic, colors represent the different pore sizes, with the real photo of the source surface area shown in the background for comparison. The image revealed abundant small pores peripherally, transitioning to sparse larger pores centrally, with negligible porosity at the

source apex. This porosity gradient, highest at the periphery and lowest at the core/top, reflected spatially heterogeneous graphitization and recrystallization. The upper-middle source region contained densely packed recrystallized SiC macroparticles underlaid by variably sized voids, beneath which acicular SiC crystals formed. This phenomenon was consistent with the simulation results on vapor transport within the powder source: on the one hand, the gaseous species that were not consumed by crystal growth transferred to the surface area of the source after strong convection, resulting in significant recrystallization on the upper surface of the source. On the other hand, due to the characteristics of downward transport of the gas phase in the upper part of the source near the center, voids formed in the lower part of the recrystallized SiC polycrystalline blocks. In addition, needle-shaped gas transport channels formed toward the source bottom and sidewalls.

The above experimental and simulation results reveal the evolution of the source during conventional PVT crystal growth. The uneven distribution of powder within the chamber significantly impacted the heat transfer characteristics of the crucible, complicating the control of the optimal thermal field distribution required for crystal growth. Key parameters, such as the axial and radial temperature gradients, were affected. Fig. S5a shows the evolution of the local temperature gradient at the central and peripheral regions of the crystal growth surface as growth progressed over time. The result revealed that the temperature gradient on the crystal growth surface steadily diminished over time. This decline weakened the driving force required for crystal growth, leading to a corresponding reduction in the crystal growth rate.[19] Moreover, the results further showed that, under the influence of the changing temperature gradient, the difference in the crystal growth rate between the center and edge areas of the crystal continued to increase (Fig. S5b). From the perspective of crystal growth evolution and growth rate, this inhomogeneous source consumption process in spatial position was not good for the stable growth of the crystal and the effective consumption of the source.

3.2. Optimized mass-transfer and source consumption using a PG plate

To address the limitations of the conventional growth chamber above, especially for the inhomogeneous source evolution caused by uneven mass transfer and strong convection, a porous graphite (PG) plate was designed in this work. This PG plate aimed to optimize the inefficient usage of the powder source and enhance the production of high-quality thick crystals. In addition to previous literature (the porous structure was used to suppress impurities and stabilize polytype,[20] improve thermal distribution, or reduce defects[21,22]), this work systematically investigates how a PG plate modifies vapor flow dynamics and thermal fields to mitigate non-uniform source consumption inside the crucible. The configuration and placement of the PG plate are illustrated in Fig. 4a. The PG plate with an inner diameter matching that of the crucible (150 mm) was positioned at 10 mm above the source material, and its thickness was set to 3 mm as a robust compromise that balances convection suppression with vapor transport (Fig. S6a). Besides its spatial structure, the porosity of the graphite plate is also a critical parameter influencing its effectiveness in modifying vapor transport and source utilization. Therefore, we conducted parameter studies on PG porosity while maintaining thermal uniformity at the seed crystal surface. These studies revealed that the average temperature at the source surface increased with rising porosity. However, the concentration of the critical vapor species SiC_2 near the growth surface of the seed crystal peaked at a porosity of 0.4 (Fig. S6b). Since effective thermal conductivity was coupled to porosity, this value reflected a clear physical balance: it preserved high axial thermal conductivity conducive to stable thermal gradients while ensuring sufficient mass permeability and retaining the ability to regulate convection. Therefore, a porosity of 0.4 was identified as the optimal value for the PG plate.

Having determined the optimal porosity of the PG plate, we next evaluated its critical influence on the thermal field distribution, a key factor governing vapor generation and transport dynamics, by comparing the structures with and without the PG under identical seed-top temperatures. As shown in Fig. 4b (initial growth stage), the optimized PG plate raised the average source chamber temperature by 15 °C and reduced the axial temperature difference in the source chamber from 95 °C to 82 °C. Crucially, Fig. 4c highlights that the most significant axial temperature gradient shifted to the graphite plates (19 °C), while the growth chamber thermal profiles remained identical between structures. Radial temperature distributions (Fig. S7) further demonstrated improved thermal homogeneity at the source top (center-edge ΔT reduced to 17 °C from 20 °C), though accompanied by a slight increase in the seed-zone gradient (15 °C *vs.* 10 °C). This overall thermal redistribution, visualized dynamically in Videos S5 and S6, is attributed to enhanced radiative heat transfer from the PG surfaces. The net effect of these thermal modifications is the obviously enhanced growth environment: the elevated source temperature markedly increases the concentration of SiC vapor species. Consequently, under the same seed-surface temperatures, the growth rate accelerates due to this rapid vapor concentration increase coupled with the stable local temperature gradient enabled by the PG structure.

In addition to modifying the thermal field, we further investigated how the PG structure impacts the vapor flow dynamics—a critical factor influencing mass transport uniformity and crystal growth stability. The modified flow-field distribution within the crucible, extracted both at the initial (0-hour) and later (168-hour) growth stages, is shown in Fig. 4d. Crucially, a direct comparison with the conventional flow field (without the PG plate, shown previously in Fig. 2b) revealed a dramatic suppression of convection. Specifically, convection within the growth chamber was greatly reduced. Quantitatively, average convective velocities decreased by approximately 26% in the source chamber and 60% in the growth chamber, respectively. However, after introducing the PG structure, the powder source maintained an impressively stable and uniform

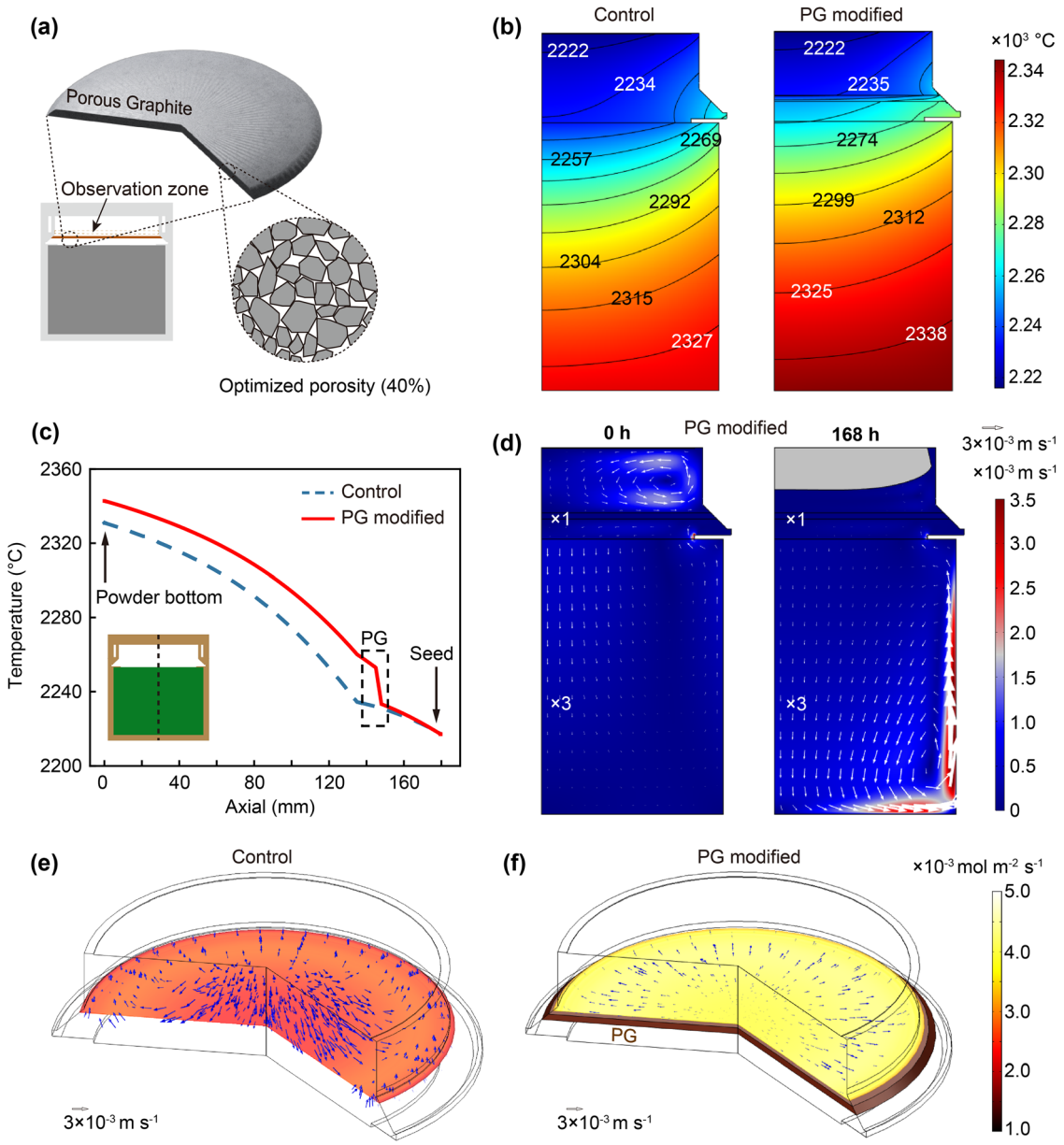

Fig. 4 (a) Schematic of PG integration in the optimized crucible. (b) Initial (0 hour) thermal field comparison between the conventional and optimized crucibles. (c) Axial temperature profiles along the crucible centerlines for both structures. (d) Comparison of velocity distributions at the 0-hour (left) and 168-h (right) growth time after adding PG, with source chamber velocities magnified 3× for clarity. 3D flow vectors (arrows) and mass flux distributions (color maps) across PG surfaces in the (e) conventional growth chamber and (f) PG-modified chamber for a comparison.

vapor supply. Even after 168 hours of growth, notable gas-phase transport persisted in the upper source region. Conversely, the conventional crucible design developed substantial recrystallization in this region due to its near-complete blockage of vapor transport. The results indicated that the PG structure effectively promoted the homogeneous sublimation of the powder source in the crucible and suppressed recrystallization at the top area of the powder source. The modified flow dynamics in 3D mode at the top area of the source for the crucible, with and without the PG plate, are visually compared in Fig. 4e and f. The PG in the optimized growth chamber reduced the source surface's average convective velocity from 1.7×10^{-3} m s^{-1} (conventional) to 4.8×10^{-4} m s^{-1}. At the same time, the net mass flux at the source surface increased by 58.3% (from 2.4×10^{-3} mol m^2 s^{-1} to 3.8×10^{-3} mol m^2 s^{-1}) for the PG-modified crucible structure. This increased net flux here meant a significantly increased crystal growth rate, which was consistent with the result of the increased surface temperature gradient of the seed crystal discussed above. Notably, similar to the recent system-level thermal-field reconstruction method,[12] the PG plate design offers an effective, alternative approach to modulate internal mass transfer and suppress recrystallization within conventional PVT setups, providing a cost-effective solution that boosts powder utilization.

3.3. Enhanced growth rate and crystal quality by the PG structure

The combined modifications to thermal distribution and flow dynamics introduced by the PG plate ultimately translate into measurable improvements in key crystal growth parameters. To comprehensively quantify these enhancements at the initial growth stage, the summary results comparing the optimized PG-modified crucible against the conventional design are presented in Fig. 5a. Notably, convection suppression was accompanied by a 30% increase in the growth rate and a ~50% enhancement in net flux. Beyond the initial growth stage, we further examined the long-term performance of the PG-modified system. The PG regulated structure maintained a growth rate increase of more than 30% compared to conventional structures (Fig. S8). In addition to the increased crystal growth rate, the thermal stress of the grown crystals was further evaluated. The equivalent 16 mm crystal thickness for the conventional structure (growth duration of 168 hours) and PG-modified structures (growth duration of 110 hours) were adopted for analysis. As quantitatively evidenced in Fig. 5b, the calculated crystal thermal stress across the 16-mm thick crystal showed an obvious decrease after introducing the PG structure. The defect density calculated based on thermal stress also showed the same trend. Crystals grown using the conventional structure showed maximum shear stress and defect density values of 13.5 MPa and 6.91 $\times$ 10^6 cm^{-2}, respectively, while the PG optimized crucible demonstrated reductions to 10.4 MPa and 3.66 $\times$ 10^6 cm^{-2} (23% and 47% decreases) despite comparable radial temperature gradients. This enhancement primarily originates from the flow-field homogenization effect induced by the PG.[23] This effect attenuates convective intensity while simultaneously improving the radial uniformity of vapor-phase component distribution. These improvements effectively suppress interfacial protrusion, as well as improve thermal distribution in the grown crystal. Consequently, thermal stress gradients are mitigated throughout the crystal volume,

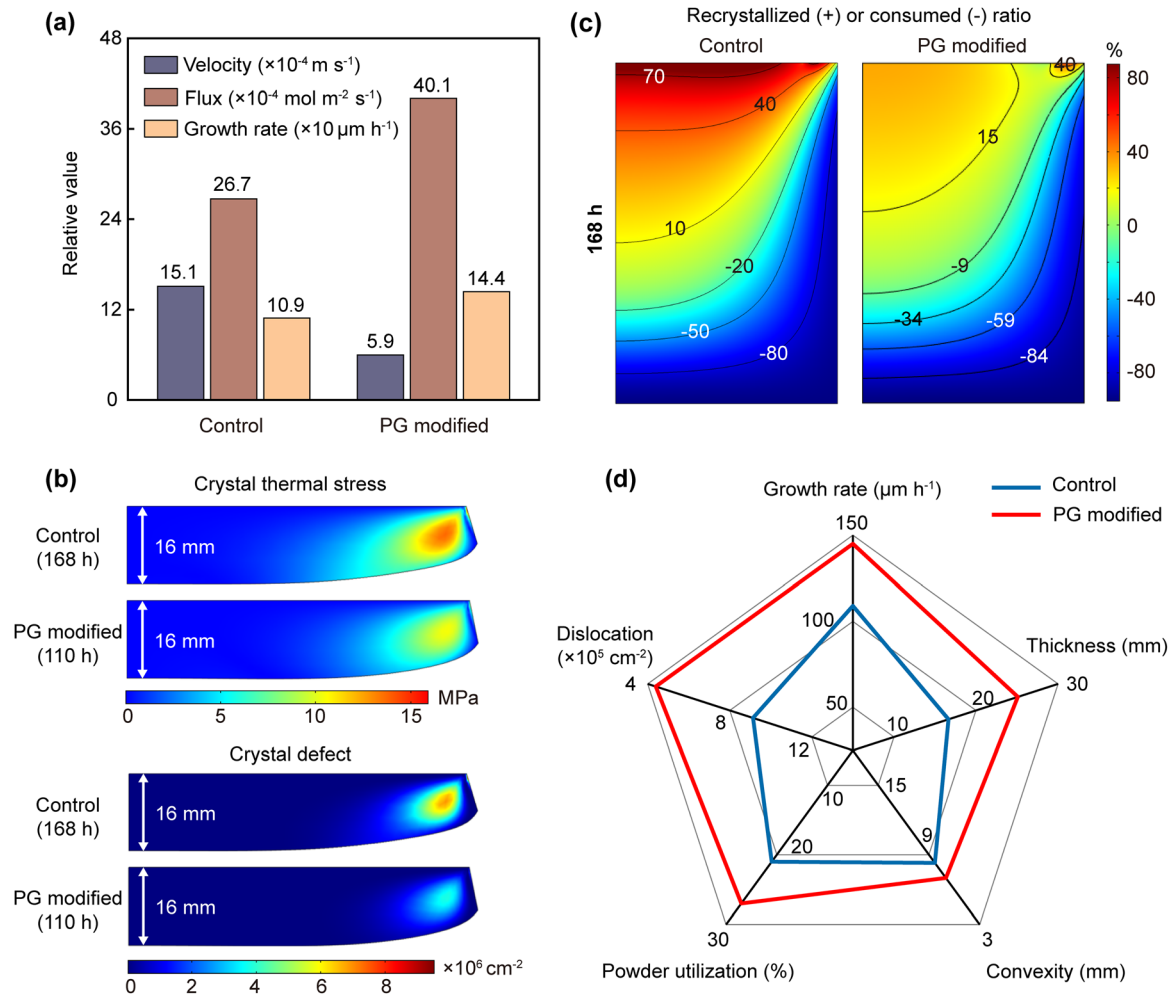

Fig. 5 (a) Comparison of the axial velocity (near the growth surface), average net flux and crystal growth rate in the control and PG-modified crucibles at the initial stage. (b) Thermal stress distribution and crystal defect density comparison between the two structures. (c) Comparison of the recrystallized (+) or consumed (–) volume ratio of the powder source for the two structures after 168-hour growth. (d) Radar chart evaluating the crystal growth rate, thickness, convexity, source utilization, and average defect density of the control and PG-modified structures.

maintaining internal shear stress below the critical resolved shear stress. This comprehensive stress management ultimately reduces crystalline defect density.[24]

Following a detailed analysis of the changes in the growth rate and quality of SiC crystals after the introduction of PG, the porosity evolution and source consumption dynamics of the SiC powder source were further investigated, as shown in Fig. S9a, b and Videos S7 and S8. Compared with the conventional structure, the PG-modified structure demonstrates a 43% reduction in the SiC recrystallization volume ratio and a 50% porosity increase at the source top region. The reduced SiC powder recrystallization can also be seen in the extracted recrystallized (+) and consumed (−) powder source volume ratio distribution patterns of the conventional and PG-modified crucibles shown in Fig. 5c. The observed improvements in source consumption for the optimized crucible structure (with PG) stem from two synergistic mechanisms. First, enhanced surface radiation due to PG elevates the source surface temperature, delivering a relatively uniform temperature distribution and more homogeneous SiC sublimation within the source region. Second, suppressed convection inside the powder source inhibits recrystallization in the upper part of the source, mitigating pore blockage and ensuring sustained gas phase transport after long-term growth. These thermal and flow-field modifications collectively mitigate spatial heterogeneity in source consumption and recrystallization, ultimately improving source utilization.

To clearly illustrate the effect of the PG plate on crystal growth, a radar chart comparing the two structures across multiple performance metrics is displayed in Fig. 5d. The results clearly indicate that the PG-modified crucible increases the growth rate by 33% relative to the conventional structure. And after 168 hours of growth, the crystal thickness achieved with the PG-modified crucible exceeded that of the conventional structure by 51%, confirming the pivotal role of PG in boosting SiC yield. Convexity, defined as the center-to-edge thickness ratio, serves as a key indicator of crystal quality. Lower convexity correlates with a flatter surface morphology, reduced thermal stress, and suppressed polycrystal/defect formation. Compared to the conventional structure, the PG structure showed an 18% reduction in convexity, resulting in a 52% lower average defect density. Furthermore, this PG structure improves the powder source utilization by 29%, where utilization is defined as the net mass of effective SiC sublimation relative to the initial loading. Specifically, utilization (%) = (total mass of sublimated powder − total mass of recrystallized SiC)/(initial mass of powder) × 100%. This improvement underscores the effectiveness of PG in minimizing material waste and production costs.

4. Conclusions

This study developed a comprehensive numerical model simulation of the source evolution coupled with heat and mass transfer dynamics during the PVT growth of SiC crystals. Through combined simulations with experimental validation, this study systematically investigated the uneven evolution of the SiC source due to graphitization and recrystallization during the growth process, with a focus on the thermal and flow fields. To address the non-uniform source consumption commonly observed in conventional growth chambers, a PG plate was specifically designed in order to optimize mass transfer in PVT chambers. This design obviously regulated the axial temperature gradient in the crucible and enhanced gas-phase convection uniformity, thus effectively suppressing source recrystallization while promoting homogeneous source consumption. The optimized process achieved simultaneous improvements in the growth rate (33% increase), source utilization (29% enhancement), and crystalline quality (52% defect reduction). The revealed source evolution mechanisms and the control strategy demonstrate a significant practical value for advancing the productivity and crystal quality of industrial SiC single crystals.

Author contributions

The manuscript was written through the contributions of all authors. All authors have given approval to the final version of the manuscript.

Conflicts of interest

There are no conflicts to declare.

Data availability

The data supporting this article have been included as part of the supplementary information (SI). Supplementary information: detailed theoretical simulation model; axial–radial thermal and flow fields in a conventional PVT crucible (Fig. S1); net flux distribution on the seed crystal surface across growth stages (Fig. S2); SiC gasification rate distribution in the initial stage (Fig. S3); comparisons between the XPS-measured and simulated powder source C/Si ratios (Fig. S4); axial temperature gradient and growth rate at seed centre *versus* edge (Fig. S5); average seed surface temperature and SiC_2 concentration *versus* porosity of PG (Fig. S6); radial temperature distribution on crucible surfaces with/without the PG plate (Fig. S7); temporal evolution of average axial temperature gradients/growth rates and their difference between structures (Fig. S8); porosity and SiC volume ratio distribution in the source chamber during growth with/without the PG plate (Fig. S9), Videos S1–S4 display reconstructed 3D CT images of full-scan cross-sections, where different shades of gray represent the density distribution of the powder source (lighter colours indicate a higher density), depicting both material density and pore volume distributions. Videos S5–S8 show the temporal evolution of the thermal field and powder volume ratio distribution with and without the PG plate. See DOI: https://doi.org/10.1039/d5ma01254f.

Acknowledgements

This work was financially supported by the National Key Research and Development Program of China (2021YFB3401604), the National Natural Science Foundation of China (62234001), the Key Scientific and Technological Program of Xiamen (3502Z2 0231045), the Innovation Program for Quantum Science and Technology (2021ZD0303400), and the Fundamental Research Funds for the Central Universities (20720240067).

References

1 A. Agarwal, M. Das, S. Krishnaswami, J. Palmour, J. Richmond and S.-H. Ryu, *MRS Online Proc. Libr.*, 2004, **815**, J1.
2 H. Daikoku, M. Kado, A. Seki, K. Sato, T. Bessho, K. Kusunoki, H. Kaidou, Y. Kishida, K. Moriguchi and K. Kamei, *Cryst. Growth Des.*, 2016, **16**, 1256–1260.
3 I.-G. Yeo, W.-S. Yang, J.-H. Park, H.-B. Ryu, W.-J. Lee, B.-C. Shin and S. Nishino, *J. Korean Phys. Soc.*, 2011, **58**, 1541–1543.
4 X. She, A. Q. Huang, O. Lucia and B. Ozpineci, *IEEE Trans. Ind. Electron.*, 2017, **64**, 8193–8205.
5 S. Zhang, H. Fu, T. Li, G. Fan and L. Zhao, *Materials*, 2022, **16**, 281.
6 R. Huang, Y. Tao, S. Bai, G. Chen, L. Wang, A. Liu, N. Wei, Y. Li and Z. Zhao, *J. Semicond.*, 2015, **36**, 094002.
7 X. Liu, B.-y Chen, L.-X. Song, E.-W. Shi and Z.-Z. Chen, *J. Cryst. Growth*, 2010, **312**, 1486–1490.
8 P. Tan, W. Kang, J. Yin and J. Kang, *Phys. Scr.*, 2022, **97**, 105708.
9 X. Wang, D. Cai and H. Zhang, *J. Cryst. Growth*, 2007, **305**, 122–132.
10 C. Zhou, Z. Lu, C. Li, Y. Lu, H. Li, L. Dong, S. Ke and S.-Y. Tong, *J. Cryst. Growth*, 2025, **668**, 128283.
11 S. Zhang, G. Fan, T. Li and L. Zhao, *RSC Adv.*, 2022, **12**, 19936–19945.
12 D. Nakamura and S.-i Nishizawa, *Appl. Phys. Express*, 2025, **18**, 105501.
13 N. Yang, B. Song, W. Wang and H. Li, *CrystEngComm*, 2022, **24**, 3475–3480.
14 S.-M. Jeong, Y.-H. Kim, J.-H. Sun, J.-H. Park, Y.-J. Shin, S.-Y. Bae, C.-M. Kim and W.-J. Lee, *CrystEngComm*, 2024, **26**, 3158–3161.
15 P. Wellmann, M. Bickermann, D. Hofmann, L. Kadinski, M. Selder, T. Straubinger and A. Winnacker, *J. Cryst. Growth*, 2000, **216**, 263–272.
16 E. Tupitsyn, A. Arulchakkaravarthi, R. Drachev and T. Sudarshan, *J. Cryst. Growth*, 2007, **299**, 70–76.
17 J. Ihle and P. J. Wellmann, *Solid State Phenom.*, 2023, **344**, 23–28.
18 A. V. Kulik, M. V. Bogdanov, S. Y. Karpov, M. S. Ramm and Y. Makarov, *Mater. Sci. Forum*, 2004, **457–460**, 67–70.
19 Q.-S. Chen, H. Zhang, V. Prasad, C. Balkas, N. Yushin and S. Wang, *J. Cryst. Growth*, 2001, **224**, 101–110.
20 H. W. Shin, H. J. Lee, H. J. Kim, D. H. Lee, M. S. Park, Y. S. Jang, W. J. Lee, I. G. Yeo, M. C. Chun, S. H. Lee and J. G. Kim, *Mater. Sci. Forum*, 2016, **858**, 113–116.
21 J.-H. Sun, J.-H. Park, S.-Y. Bae, Y.-J. Shin, Y.-J. Kwon, W.-J. Lee, S.-H. Kwon and S.-M. Jeong, *Materials*, 2024, **17**, 5789.
22 T. Wei, H. Guo, Q. Shao, D. Yang, X. Pi and L. Xu, *Ceram. Int.*, 2025, **51**, 29457–29464.
23 Y. Yang, T. Lin and Z. Chen, *J. Semicond.*, 2008, **29**, 851–854.
24 X. Ye, A. Zhang, J. Huang, W. Kang, W. Jiang, X. Li, J. Yin and J. Kang, *Aggregate*, 2024, **5**, e524.